General Parameterized Time-Frequency Transform

Y. Yang, Z. K. Peng, X. J. Dong, W. M. Zhang, *Member, IEEE*, and G. Meng

***Abstract*—Interest in parameterized time-frequency analysis for non-stationary signal processing is increasing steadily. An important advantage of such analysis is to provide highly concentrated time-frequency representation with signal-dependent resolution. In this paper, a general scheme, named as general parameterized time-frequency transform (GPTF transform), is proposed for carrying out parameterized time-frequency analysis. The GPTF transform is defined by applying generalized kernel based rotation operator and shift operator. It provides the availability of a single generalized time-frequency transform for applications on signals of different natures. Furthermore, by replacing kernel function, it facilitates the implementation of various parameterized time – frequency transforms from the same standpoint. The desirable properties and the dual definition in the frequency domain of GPTF transform are also described in this paper. One of the advantages of the GPTF transform is that the generalized kernel can be customized to characterize the time – frequency signature of non-stationary signal. As different kernel formulation has bias toward the signal to be analyzed, a proper kernel is vital to the GPTF. Thus, several potential kernels are provided and discussed in this paper to develop the desired parameterized time – frequency transforms. In real applications, it is desired to identify proper kernel with respect to the considered signal. This motivates us to propose an effective method to identify the kernel for the GPTF.**

***Index Terms*—General parameterized time-frequency transform, kernel formulation, time frequency analysis, time-frequency concentration.**

I. Introduction

In signal processing discipline, Fourier transform is known as a powerful tool of revealing the overall spectral contents by assuming the given signal is a stationary time series. However, it has been well recognized that the concept of stationary time series is an ideal assumption and not particularly useful in practice. For instance, when a rotary machine, i.e., helicopter rotor, wind turbine, hydraulic turbine, is operating under time – varying rotational speed, the frequency components of vibration signal are strongly dependent on time. Another example from speech recognition is that the frequencies of human speech evolve over time depending on the pronounced words or syllables. Clearly, for these non-stationary signals, Fourier transform is insufficient. Thus, it is desirable to resort to time – frequency representation (TFR) that represents the energy density of a signal simultaneously in time–frequency plane. A better concentrated TFR is expected to be able to characterize the time-frequency signature of the considered signal more accurately. Usually, two parameters are used to quantify the time – frequency signature of mono-component non-stationary signal, i.e., instantaneous frequency and localized frequency delay [1], [2]. Mathematically, the former is a function of time while the latter is a function of frequency.

Traditional techniques of obtaining TFR include short-time Fourier transform (STFT), wavelet transform (WT), and Wigner-Ville distribution (WVD). Specifically, STFT divides a non-stationary signal into blocks of short, pseudo-stationary segments, with fixed Gaussian window. The window width controls the tradeoff of bias and variance. Shorter window leads to poor frequency resolution, while longer window improves the frequency resolution but compromises the stationary assumption within this window. To deal with the local resolution requirement, various adaptive methods have been designed for STFT. For example, the window width is adjusted depending on the given signal instead of constant-width (e.g., see [3]–[8]). From an approximation point of view, the STFT is a piece-wise zero-order fitting of signal in the time-frequency plane. It is not a good choice to analyze the non-stationary signal whose spectral component varies over time. Alternatively, WT projects signal into a class of wavelets that is generated by a "mother wavelet". As long as one class of wavelet function is developed, a new WT is proposed (e.g., see [9]–[11]). From a point view of window – based analysis, WT is adaptive due to the usage of scale factor (corresponding to wavelet width) that is inversely proportional to the frequency of the given signal. The Heisenberg uncertainty principle states that the time and the frequency resolution of a time-frequency transform cannot reach the best at the same time. In the case of WT, its results have higher frequency resolution and lower time resolution for lower frequency components while have lower frequency resolution and higher time resolution for higher frequency components. However, the frequency resolution at the same scale level cannot be adaptively adjusted. Although STFT and WT are different in the usage of transform basis, they all essentially use horizontal lines to approximate the instantaneous frequency (IF) trajectory of the given signal in the time-frequency plane. Thus, the TFR concentration cannot be significantly improved for non-stationary signal with rapidly time-varying frequency component. In comparison, WVD, basically the Fourier transform of instantaneous autocorrelation function of a signal, is a representative

Manuscript received July 22, 2013; revised January 26, 2014 and March 17, 2014; accepted March 23, 2014. Date of publication March 26, 2014; date of current version May 05, 2014. The associate editor coordinating the review of this manuscript and approving it for publication was Prof. Antonio Napolitano. This work was supported by the NSFC for Distinguished Young Scholars (11125209), the Excellent Young Scholars (11322215), and the NSFC (51121063, 11072147).

The authors are with the State Key Laboratory of Mechanical System and Vibration, Shanghai Jiao Tong University, Shanghai 200240, P.R. China (e-mail: emma002@sjtu.edu.cn; z.peng@sjtu.edu.cn; donxij@sjtu.edu.cn; wenmingz@sjtu.edu.cn; gmeng@sjtu.edu.cn).

This paper has supplementary downloadable multimedia material available at http://ieeexplore.ieee.org provided by the authors. This material is 16 KB in size.

Color versions of one or more of the figures in this paper are available online at http://ieeexplore.ieee.org.

Digital Object Identifier 10.1109/TSP.2014.2314061

of bilinear time-frequency analysis. An advantage of WVD is that it could generate TFR with the high concentration, though it inevitably introduces plenty of cross-terms. To suppress the cross-terms, various methods have been proposed (e.g., see [12]–[14]). The dominant question focuses on how to carefully balance the tradeoff between cross-terms suppression and TFR concentration. The aforementioned methods are referred to as non-parameterized time-frequency analysis as they all use the signal-independent parameter, i.e., window length or lag (used to calculate instantaneous autocorrelation in WVD). In general, these non-parameterized time-frequency methods cannot provide high-quality TFR for non-stationary signal. From a point view of post-processing, reassignment method was put forward by Auger and Flandrin to improve the readability of TFR [15], [16]. The reassignment is realized by assigning the average of energy in a domain to the gravity center of these energy contributions. It reduces energy spread of TFR at the cost of greater computational complexity. In the case of noise, the reassignment technique inevitably introduces interference terms since the computed gravity center unnecessarily represents the real energy distribution of the interested signal.

The time-frequency methods, which use extra signal- dependent parameters, are referred to as parameterized time-frequency analysis. It attracts considerable attention because of the signal-dependent resolution and highly concentrated TFR. The best-known example is "chirplet transform", which was proposed by Mann and Haykin [17], Milhovilovic and Bracewell [18] almost at the same time. It projects a signal into a family of chirplets that is obtained through translating, scaling, and shearing a "mother chirplet". The chirplet is an atom which is specially designed for linear modulated signal analysis. By using an extra parameter, chirp rate, the chirplet transform is able to obtain a well concentrated TFR. For the sake of argument, we denote the standard chirplet transform as a transform that uses a unified chirp rate, and chirplet decomposition as a method that selects a group of optimal chirplets from a pre-defined atom dictionary. The former represents the IF of signal with a line of arbitrary slope in the time-frequency plane, while the latter uses a group of lines. Specially, the chirplet decomposition is usually realized by using matching pursuit algorithm (e.g., see [19], [20]). Nevertheless, due to the nature of linear approximation, neither of them is suitable to analyze nonlinear frequency-modulated signal.

To deal with such signals, an intuitive solution is to adaptively approximate the local signal with chirplets (e.g., see [21]–[25]). Cui and Wong [26] developed an adaptive windowed chirplet decomposition method. It divides signal into blocks of short that can be approximated by different chirplets. They further proposed a scheme to determine the optimal division [27]. Chassande-Mottin and Pai [28] proposed an algorithm to search the best chirplet chain according to the time-frequency signature of the signal. Dugnol *et al.* [29] proposed another adaptive method that is required to determine whether the consecutive optimal chirplets belong to the same component. Candes *et al.* [30] proposed chirplet path pursuit method to detect highly oscillatory signals. It applies locally well correlated chirplets of compact supported for the approximation purpose. Since the search process requires expensive computation, Gribonval [31] proposed modified matching pursuit algorithm, named fast ridge pursuit, to get a fairly "good" chirplet. Its acceleration dependents on the sub-dictionary of Gabor atom selected at the first stage. In the case of signals with strong nonlinear time-frequency signature, a large amount of chirplets is required to accurately approximate the signal. The computation complexity of such requirement would make these methods suffer.

In order to accurately characterize the nonlinear instantaneous frequency of a signal, some attempts focus on constructing well localized atoms through modifying the chirplet. For example, Angrisani and D'Arco [32] proposed a modified version of chirplet with additional bending factor. Papandreou-Suppappola and Suppappola [33] constructed a dictionary consisted of nonlinear frequency modulated chirplet. To deal with signals with strong local nonlinear time-frequency pattern, Dopplerlet transform [34] and $\mathrm{FM}^m\mathrm{let}$ transform [35] have been proposed. They are all implemented by matching pursuit algorithm. The former uses Doppler function as the mother function, named Dopperlet, and the latter introduces an exponent into the chirplet, named $\mathrm{FM}^m\mathrm{let}$. Despite this, most of these methods are based on maximum likelihood criterion and realized by greedy search, which is sensitive to noise and time-consuming.

To efficiently implement parameterized time-frequency transform, alternative schemes have been proposed recently. For instance, Katkovnik [36] proposed local polynomial Fourier transform (LPFT), which is generalized STFT. Particularly, LPFT uses polynomial to fit local nonlinearly time-varying instantaneous frequency. It generates TFR over a space of time versus the instantaneous frequency and its derivatives. Later, we proposed polynomial chirplet transform (PCT) [37] implemented by a polynomial kernel-based scheme, which is derived from standard chirplet transform. Essentially, it approximates the IF trajectory of the given signal with a polynomial function. However, the polynomial is not always a perfect approximation. In the case of highly oscillating instantaneous frequency, lower order polynomial is too smooth to fit accurately, while higher order polynomial approximation suffers from "Runge" phenomenon, which is a problem of oscillation at the edges of an approximation interval. To analyze the signal whose IF trajectory cannot be approximated by a polynomial, we then proposed spline chirplet transform (SCT) [38]. It is different from the PCT in using spline kernel function. For a special class of signals with periodical time-varying instantaneous frequency, Angrisani *et al.* [39] proposed warblet transform in which a set of basis with modulated by trigonometric function of time is adopted. However, it is not suitable to analyze signals with non-periodical time-varying instantaneous frequency. To expand applications of the warblet transform, we proposed generalized warblet transform (GWT) [40] by using Fourier series kernel.

At this point, several interesting questions may arise:

1) Are the PCT, SCT and GWT included by a general transform, which is available to analyze signals of different natures?
2) What is the foundation of such a transform and how can it be constructed?

3) If such a transform exists, does it include other existing time-frequency transforms as special cases, or is there a general scheme to develop new parameterized time-frequency transforms? If so, how to formulate a desired time-frequency transform?

The above questions imply the main purpose of our paper: to lay down the general scheme for parameterized time-frequency transform. It is promising to become a general framework that can implement various time-frequency transforms, i.e., STFT, chirplet transform, $\mathrm{FM}^m\mathrm{let}$ transform, warblet transform, PCT, SCT, GWT and so on, from a unified standpoint.

Towards this goal, we introduce general parameterized time-frequency transform (GPTF transform). The remainder of this paper includes five sections totally.

Sections II and III mainly focus on the definition of the GPTF transform. Specifically, as the main components to construct the GPTF are kernel-based rotation operator and shift operator, Section II emphasize on the development of these two operators by rewriting a standard chirplet transform. Most details of the GPTF transform are further provided in Section III: 1) in Part A, the GPTF transform is defined through integrating an arbitrary integrable kernel function into the two operators; 2) in Part B, several important properties of the defined GPTF transform are discussed, i.e., linearity, scaling, time shifting and frequency shifting properties; 3) in Part C, the dual definition of the GPTF transform in frequency domain, a counterpart of the GPTF transform in time domain, is provided.

Sections IV and V are assigned to discuss the formulation and identification problem for the kernel of the GPTF transform. As different kernel formulation has bias toward the signal to be analyzed, a proper kernel is vital to the GPTF. In order to develop a desired parameterized time – frequency transform, several potential kernels are provided and discussed in Section IV. Furthermore, it is important to identify the kernel with respect to the considered signal in real applications. Thus, an effective method is needed to identify the proper kernel for a GPTF transform. To fulfill this task, a recursive IF approximation based kernel identification method is addressed in Section V. Finally, Section VI concludes the paper.

II. Rotation and Shift Operators

Chirplet transform is widely used to analyze linear frequency modulated signal. For a signal $s(t) \in L^2(R)$, the chirplet transform is defined as [17], [29]

$$CT_s\left(t_0,\omega,\alpha;\sigma\right)=\int_{-\infty}^{+\infty} z(t)\Psi^*_{(t_0,\alpha,\sigma)}(t)e^{-j\omega t}dt \quad (1)$$

where $z(t)$ is the analytical signal of $s(t)$, generated by Hilbert transform, $\boldsymbol{H}$, i.e., $z(t)=s(t)+j\boldsymbol{H}[s(t)]$, and $\Psi_{(t_0,\alpha,\sigma)}(t)$ is a complex window.

$$\Psi_{(t_0,\alpha,\sigma)}(t)=w_\sigma(t-t_0)e^{j\frac{\alpha}{2}(t-t_0)^2} \quad (2)$$

in which parameters t_0, $\alpha \in R$ stand for time and chirp rate respectively; $w \in L^2(R)$ denotes a non-negative, symmetric and normalized real window. If it is taken as a Gaussian function,

$$w_\sigma(t)=\frac{1}{\sqrt{2\pi}\sigma}e^{-\frac{1}{2}(t/\sigma)^2}. \quad (3)$$

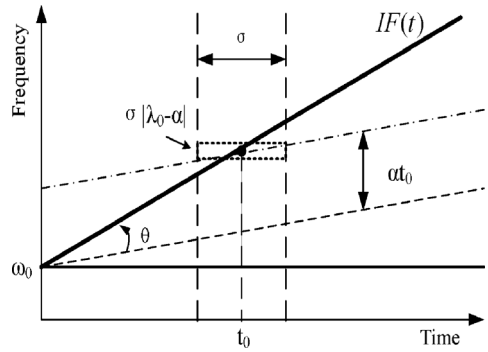

Fig. 1. An illustration of rotation operator and shift operator (□ — the IF law of the object signal; - — after frequency rotation; -. — after frequency shift).

where σ is window length, (2) will be referred to Gaussian chirplet transform.

According to(1), the chirplet transform is essentially STFT of the analytical signal multiplied by the complex window $\Psi^*_{(t_0,\alpha,\sigma)}(t)$. By manipulating (1), chirplet transform can also be written as

$$CT_s(t_0,\omega,\alpha;\sigma)=A(t_0)\int_{-\infty}^{+\infty}\overline{z}(t)w_\sigma(t-t_0)e^{-j\omega t}dt \quad (4)$$

with

$$\begin{cases}\overline{z}(t)=z(t)\Phi^R_\alpha(t)\Phi^S_\alpha(t,t_0)\\ \Phi^R_\alpha(t)=e^{-j\alpha t^2/2}\\ \Phi^S_\alpha(t,t_0)=e^{j\alpha t_0 t}\\ A(t_0)=e^{-jt_0^2\alpha/2}\end{cases}$$

where $|A(t_0)|=1$; α is the chirp rate. Here, we define $\Phi^R_\alpha(t)$ and $\Phi^S_\alpha(t,t_0)$ are *rotation operator* and *shift operator*, respectively.

For a linear modulated signal which is given by

$$s\left(t\right)=Ae^{j\left(\omega_0 t+\lambda_0 t^2/2\right)} \quad (5)$$

where ω_0 denotes initial frequency; λ_0 is chirp rate. Its instantaneous frequency (IF) law is $IF\left(t\right)=\omega_0+\lambda_0 t$. The functionality of these two operators is illustrated in Fig. 1. In this figure, $\Phi^R_\alpha(t)$ rotates the analytical signal $z(t)$ by an angle θ with $tg(\theta)=-\alpha$ in time-frequency plane; $\Phi^S_\alpha(t,t_0)$ relocates a frequency component of ω at t_0 to $\omega+\alpha t_0$. Therefore, chirplet transform can be reinterpreted as three operations: 1) rotating a signal by a degree $\arctan(-\alpha)$ in time-frequency plane; 2) shifting the signal by a frequency increment of αt_0; 3) doing standard STFT with window $w_\sigma\left(t\right)$.

The signal-dependent frequency resolution of chirplet transform can be easily determined from Fig. 1. It can be seen that the frequency bandwidth of the windowed signal segment is $\sigma\left|\lambda_0-\alpha\right|+1/\sigma$ and the time bandwidth is σ. When $\alpha=\lambda_0$, the frequency resolution will reach the minimum, $1/\sigma$. As a result, $|CT_s(t_0,\omega,\alpha;\sigma)|$ achieves the global maximum at $(\omega,\alpha)=(\omega_0+\lambda_0 t_0,\lambda_0)$. It implies that chirplet transform could generate a best concentrated TFR with proper chirp rate.

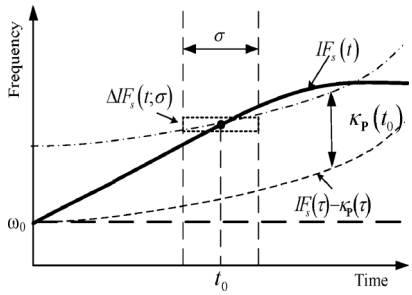

Fig. 2. Principle of parameterized time-frequency analysis.

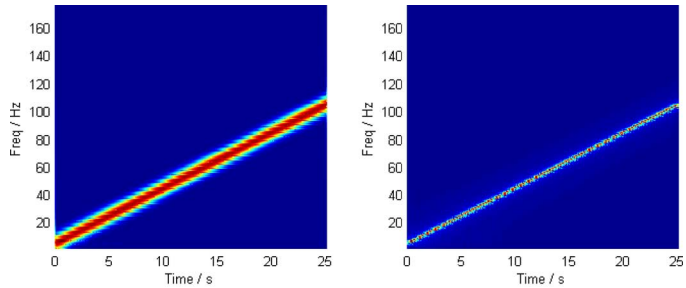

Fig. 3. Window size effect on GPTF. (a) window size: 128. (b) window size: 2048.

III. General Parameterized Time-Frequency Transform

Definition

According to (4), the chirplet transform can be implemented with a scheme based on the *rotation operator* and *shift operator*. Basically, the *rotation/shift operator* rotates/shifts the signal of any time with subtracting/adding the same amount, αt, in time-frequency plane. It implies that these operators can be constructed with the same kernel. With the help of chirp rate, chirplet transform is able to characterize the linear IF of linear modulated signal. However, it is not always applicable.

For any signal, such as

$$z(t) = Ae^{j\int IF(t)dt} \tag{6}$$

whose time-frequency signature is characterized by any arbitrary IF, $IF(t)$.Therefore, to deal with such signal, we define general parameterized time-frequency transform (GPTF transform) as

$$TF_s(t_0,\omega;\mathbf{P}) = \int_{-\infty}^{+\infty} \overline{z}(\tau)\, w_\sigma^*(\tau - t_0)\, e^{-j\omega\tau} d\tau \tag{7}$$

with

$$\begin{cases} \overline{z}(\tau) = z(\tau)\,\Phi_{\mathbf{P}}^R(\tau)\,\Phi_{t_0,\mathbf{P}}^S(\tau) \\ \Phi_{\mathbf{P}}^R(\tau) = e^{-j\int \kappa_{\mathbf{P}}(\tau)d\tau} \\ \Phi_{t_0,\mathbf{P}}^S(\tau) = e^{j\tau\cdot\kappa_{\mathbf{P}}(t_0)} \end{cases}$$

In (7), $\Phi_{\mathbf{P}}^R(t)$ and $\Phi_{t_0,\mathbf{P}}^S(t)$ denote the kernel-based *rotation operator* and *shift operator* in GPTF transform, respectively; $\kappa_{\mathbf{P}}(t)$ is an integrable kernel function; $\mathbf{P}$ denotes parameter set.

Similarly, GPTF transform contains three operators. Fig. 2 illustrates the procedure of GPTF transform. In time-frequency plane, the signal with instantaneous frequency of $IF_s(t)$ is first rotated by subtracting $\kappa_{\mathbf{P}}(t)$ at any time, then it is shifted by $\kappa_{\mathbf{P}}(t_0)$ at each time of t_0 and STFT is finally performed with the window of $w_\sigma(t)$. Clearly, the GPTF transform provides the availability of a single generalized time-frequency transform for applications on signals of different natures. Particularly, when $\kappa_{\mathbf{P}}(t) \equiv 0$, the GPTF transform will equal to standard STFT; when $\kappa_{\mathbf{P}}(t) = \alpha t$, the GPTF transform will be equivalent to chirplet transform.

The contributions of kernel function, $\kappa_{\mathbf{P}}(t)$, to frequency resolution can be analyzed according to Fig. 2. From another point of view, the GPTF transform has time-frequency plane tiled in a fashion of enclosed area, i.e., rectangular in the case of $\kappa_{\mathbf{P}}(t) \equiv 0$. Each enclosed area is called time-frequency cell, whose length and width are time resolution and frequency resolution, respectively. The frequency resolution of the GPTF transform depends on two ingredients: 1) the bandwidth of the windowed signal after rotation and shift, denoted as $\Delta IF_s(t_0;\sigma)$; 2) the bandwidth of analysis window, which will be $1/\sigma$ when Gaussian window is adopted. To sum up, the frequency resolution of GPTF transform equals the $\Delta IF_s(t_0;\sigma)+1/\sigma$. When the parameter set is properly determined, kernel function will be closely approximated to real IF. In this case, $\Delta IF_s(t_0;\sigma)$ equals the zero and the frequency resolution reaches the minimum of $1/\sigma$. Therefore, GPTF transform is able to provide signal-dependent frequency resolution.

From the energy point of view, When the kernel has been properly determined, the IF of signal will be rotated to be a constant, ω_0, at any time instance using the *rotation operator*. As a result, the energy of the windowed signal will focus at the center of time-frequency cell. Then, the *shift operator* is only responsible for moving the energy of the rotated signal to the real IF trajectory controlled by the kernel function in time-frequency plane. It implies that the overall concentration of GPTF transform is essentially determined by the concentration of rotated signal. It can be explained from Fig. 2.

For the signal with continuous IF, the signal rotated with the matched kernel can be considered to be stationary. At this point, the ultimate performance of the GPTF is the same with the resolution of the STFT on the rotated signal, which prefers the longer observation duration (longer window) to attain the better frequency resolution. In other words, the better TFR can be achieved by the GPTF with the longer window. Fig. 3 provides a simple example with the linear modulated signal. The sampling frequency is 500 Hz, and the window size is set to 128 and 2048 respectively. Here, the GPTF transform applies a linear kernel. It can be seen that the short window results in the energy smeared along the frequency axis, while the long window achieves the better concentration. On the other hand, for the signal with discontinuous IF, the window length has to be limited to balance the tradeoff between the time and frequency resolutions.

The paper is innovative in two aspects: 1) providing a single generalized TFR for applications on signals of different natures; 2) using an arbitrary integrable kernel function that can be replaced to implement diverse parameterized time-frequency transforms.

A. Properties

Through the GPTF transform, any analytical signal of $z(t)$ can be represented in its parameterized TFR, i.e.,

$$z(t) \xrightarrow{\text{GPTF transform}} TF_z(t,\omega;\mathbf{P}) = \int_{-\infty}^{+\infty} \overline{z}(\tau)\, w_\sigma^*(\tau - t)\, e^{-j\omega\tau} d\tau \quad (8)$$

Here, we investigate how the operation of signal in the time domain affects its parameterized TFR. Based on the GPTF transform defined in (7), several properties can be derived as follows.

1) Linearity Property: Assuming there are two signals $z_1(t)$ and $z_2(t)$, as well as two arbitrary constants of m and n, their GPTF transforms are given by

$$z_1(t) \xrightarrow{\text{GPTF transform}} TF_{z_1}(t,\omega;\mathbf{P})$$
$$z_2(t) \xrightarrow{\text{GPTF transform}} TF_{z_2}(t,\omega;\mathbf{P})$$

Then the GPTF transform of signal $mz_1(t)+nz_2(t)$ is given by

$$mz_1(t) + nz_2(t) \xrightarrow{\text{GPTF transform}} m \cdot TF_{z_1}(t,f;\mathbf{P}) + n \cdot TF_{z_2}(t,f;\mathbf{P}) \quad (9)$$

The linearity property can be straightforwardly proved by the linearity property of inner product. It implies the linear nature of GPTF transform.

2) Scaling Property: Assuming $\rho > 0$, then

$$z(\rho t) \xrightarrow{\text{GPTF transform}} \frac{1}{|\rho|} TF_z\left(\rho t, \frac{\omega}{\rho};\mathbf{P}\right) \quad (10)$$

Proof:

$$\begin{aligned} &TF_{z(\rho t)}(t,\omega;\mathbf{P}) \\ &\quad = \int_{-\infty}^{+\infty} \overline{z}(\rho\tau)\, w_\sigma^*(\tau - t)\, e^{-j\omega\tau} d\tau \\ &\quad \underline{\underline{\upsilon = \rho\tau}}\ \frac{1}{|\rho|} \int_{-\infty}^{+\infty} \overline{s}(\upsilon)\, w_\sigma^*\left(\frac{\upsilon - \rho t}{\rho}\right) e^{-j\frac{\omega}{\rho}\upsilon} d\upsilon \\ &\quad = \frac{1}{|\rho|} TF_z\left(\rho t, \frac{\omega}{\rho};\mathbf{P}\right) \end{aligned}$$

The scaling property indicates that when the signal is compressed in time domain by $1/\rho$ times, its parameterized TFR will be stretched along the frequency axis by ρ times and the corresponding amplitude will be reduced by $1/|\rho|$ times.

3) Time Shifting Property: Assuming $t_0 \in R$, then

$$z(t - t_0) \xrightarrow{\text{GPTF transform}} e^{-j\omega t_0} TF_z(t - t_0, \omega;\mathbf{P}) \quad (11)$$

Proof:

$$\begin{aligned} &TF_{z(t-t_0)}(t,\omega;\mathbf{P}) \\ &\quad = \int_{-\infty}^{+\infty} \overline{z}(\tau - t_0)\, w_\sigma^*(\tau - t)\, e^{-j\omega\tau} d\tau \\ &\quad \underline{\underline{\upsilon = \tau - t_0}} \int_{-\infty}^{+\infty} \overline{z}(\upsilon)\, w_\sigma^*[\upsilon - (t - t_0)]\, e^{-j\omega(\upsilon + t_0)} d\upsilon \\ &\quad \underline{\underline{\upsilon = \tau - t_0}}\ e^{-j\omega t_0} \int_{-\infty}^{+\infty} \overline{z}(\upsilon)\, w_\sigma^*[\upsilon - (t - t_0)]\, e^{-j\omega\upsilon} d\upsilon \\ &\quad = e^{-j\omega t_0} TF_z(t - t_0, \omega;\mathbf{P}) \end{aligned}$$

The time shifting property indicates that when the signal is shifted by t_0 ($t_0 > 0$) in the time domain, its frequency contents in parameterized TFR will be delayed by the amount that is proportional to f_c , i.e., $2\pi f_c t_0$, and remain the same amplitude.

4) Frequency Shifting Property: Assuming $f_0 \in \mathrm{R}$, then

$$z(t)\, e^{j\omega_0 t} \xrightarrow{\text{GP transdform}} TF_z(t, \omega - \omega_0;\mathbf{P}) \quad (12)$$

Proof:

$$\begin{aligned} TF_{z(t)e^{j\omega_0 t}}(t,\omega;\mathbf{P}) &= \int_{-\infty}^{+\infty} \overline{z}(\tau)\, e^{j\omega_0 t} w_\sigma^*(\tau - t)\, e^{-j\omega\tau} d\tau \\ &= \int_{-\infty}^{+\infty} \overline{z}(\tau)\, w_\sigma^*(\tau - t)\, e^{-j(\omega - \omega_0)} d\tau \\ &= TF_z(t, \omega - \omega_0;\mathbf{P}) \end{aligned}$$

The frequency shifting property indicates that multiplying $e^{j\omega_0 t}$ to the time-domain signal is equivalent to shift it in parameterized TFR along the frequency axis by ω_0.

B. Dual Definition in Frequency Domain

Non-destructive evaluation based on guided wave arises more attentions recently. The guided wave is a typical dispersive signal, whose group velocity changes with wave frequency. Effective applications of the guided wave depend on group velocity dispersion feature, which is convertible with localized frequency delay (LFD) in TFR. The LFD indicates the time delay of the received wave depending on its frequency.

In order to deal with such signal effectively, the dual definition of GPTF transform in frequency domain is given by

$$FTF_{\hat{s}}(t,\omega_0;\mathbf{Q}) = \frac{1}{2\pi} \int_{-\infty}^{+\infty} \overline{Z}(\theta)\, \hat{w}_\sigma^*(\theta - \omega_0)\, e^{-j\theta t} d\theta \quad (13)$$

with

$$\begin{aligned} \overline{Z}(\theta) &= \hat{s}(\theta) \cdot \Gamma_{\mathbf{Q}}^R(\theta) \cdot \Gamma_{\omega_0,\mathbf{Q}}^S(\theta) \\ \Gamma_{\mathbf{Q}}^R(\theta) &= e^{-j\int \gamma_{\mathbf{Q}}(\theta) d\theta} \\ \Gamma_{\omega_0,\mathbf{Q}}^S(\theta) &= e^{j\theta \cdot \gamma_{\mathbf{Q}}(\omega_0)} \end{aligned}$$

Here, the symbol of "$\hat{}$" denotes Fourier transform; $\Gamma_{\mathbf{Q}}^R(\omega)$ and $\Gamma_{\omega_0,\mathbf{Q}}^S(\omega)$ represent LFD *rotation operator* and *shift operator*, respectively; $\gamma_{\mathbf{Q}}(\omega)$ is an integrable kernel function of frequency.

Similar to its definition in the time domain, the dual definition of the GPTF transform is consisted of three ingredients. The difference is that the latter uses the kernel function of frequency to construct the *rotation operator* and *shift operator*, and does short-frequency Fourier transform instead. The contributions of kernel, $\gamma_{\mathbf{Q}}(\omega)$, to time/frequency resolution can be also analyzed according to Fig. 2. In this case, the time and frequency axes need to be exchanged. The detail of this analysis is unanimous to its counterpart in Section III-A.

IV. Kernel Formulation

One of interesting merits of GPTF transform is the generalized platform provided to obtain TFR for signals with different natures. Thus, it is expected to develop diverse time-frequency transforms by replacing the kernel function for various signal processing tasks. A proper kernel could fulfill the concentration requirement of TFR. In contrary, an inappropriate kernel

TABLE I
COMMONLY USED KERNEL FUNCTION

	$\kappa_{\mathbf{P}}(t)$	$\gamma_{\mathbf{Q}}(\omega)$
Short-time Fourier transform(STFT)	0	
Short-frequency Fourier transform(SFFT)		0
Chirplet transform	αt	
Warblet transform	$\cos(\overline{\omega} t)$	
FM^{m}let transform	$(1+\alpha t)^m$	

would jeopardize the TFR. Generally, a proper kernel means that it could approximately characterize the time-frequency signature of the interested signal. However, different kernel forms have bias towards the signal to be analyzed. For instance, linear kernel function is not suitable to analyze nonlinear modulated signal. Sometimes, no matter how to select the parameters, the kernel still cannot closely fit the time-frequency signature of the given signal. Therefore, the kernel formulation is a key step to develop a promising parameterized time-frequency transform.

On the one hand, several common time-frequency transforms can be viewed as special cases of GPTF transform with different kernel function. The kernel functions of these time-frequency transforms are listed in Table I, in which $\overline{\omega}$ denotes the frequency modulation parameter of the warblet transform; m represents the exponent that is used to construct $\mathrm{FM}^m\mathrm{let}$.

On the other hand, potential kernels can also be formulated based on the condition of curve fitting and prior knowledge about the signal in practice. In the same way, the developed transform is limited by the fitting condition of kernel function. To demonstrate this concept, through defining different kernel formulations, we have developed several parameterized time-frequency transforms based on the GPTF transform for different signal processing tasks. As for the topic of kernel identification, interested reader can refer to the sequel.

A. Polynomial Chirplet Transform [37]

The Weierstrass approximation theorem, in mathematics, guarantees that any continuous function on a bounded interval can be uniformly approximated by a polynomial to any degree of accuracy [41]. Thus, the polynomial kernel is optional for a wide range of signals with IF trajectories being any continuous functions of time. In order to deal with such signal, we replace the kernel with a polynomial function as

$$\kappa_{\mathbf{P}}(t) = \sum_{i=2}^{n+1} c_{i-1} t^{i-1} \tag{14}$$

where $\{c_1, \ldots, c_n\}$ denotes the polynomial coefficients. Substituting (14) into (7), we can obtain

$$\begin{aligned} &PCT_s(t_0, \omega; c_1, \ldots, c_n) \\ &= \int_{-\infty}^{+\infty} z(\tau)\, \Phi^R_{c_1,\ldots,c_n}(\tau) \Phi^S_{t_0,c_1,\ldots,c_n}(\tau)\, w^*_\sigma(\tau - t)\, e^{-j\omega\tau} d\tau \\ &\Phi^R_{c_1,\ldots,c_n}(\tau) = e^{-j\sum_{i=2}^{n+1} \frac{1}{i} c_{i-1} \tau^i} \\ &\Phi^S_{t_0,c_1,\ldots,c_n}(\tau) = e^{j\sum_{i=2}^{n+1} c_{i-1} t_0^{i-1} \tau} \end{aligned} \tag{15}$$

which is named polynomial chirplet transform (PCT).

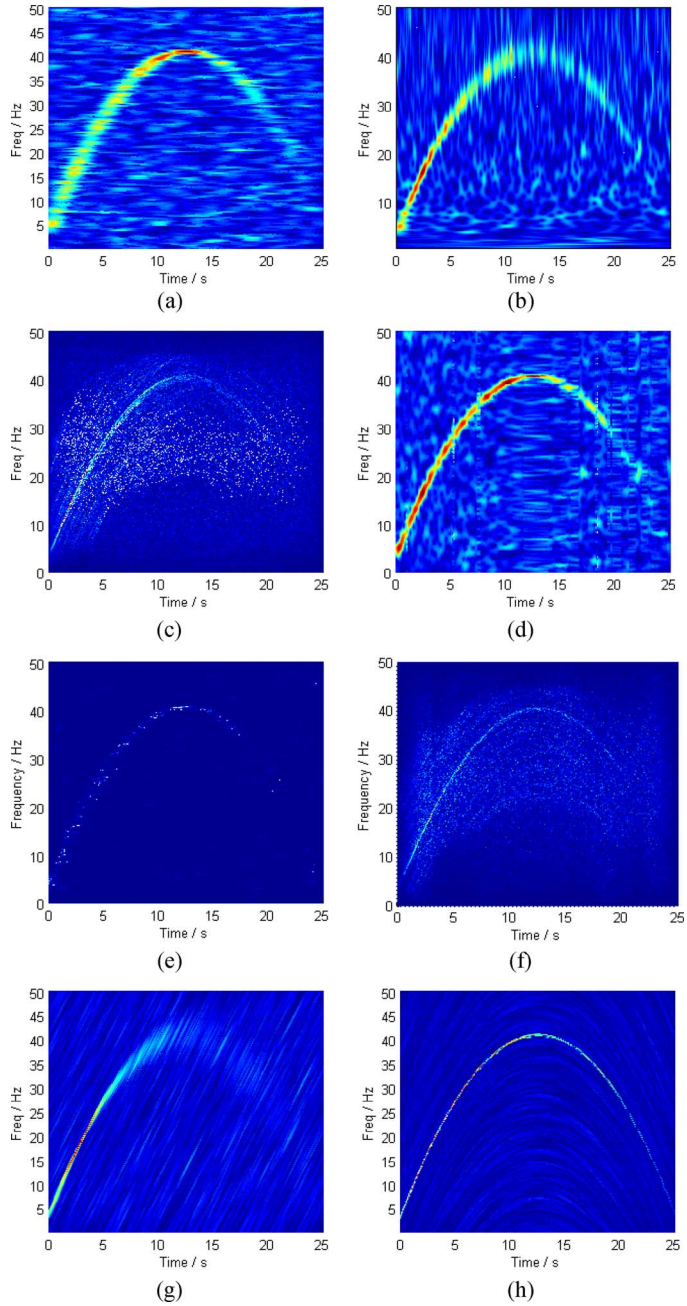

Fig. 4. TFRs of the signal in (16). (a) STFT. (b) wavelet transform. (c) WVD. (d) ASTFT. (e) reassigned spectrogram. (f) reassigned pseudo WVD. (g) chirplet transform. (h) PCT.

To demonstrate the advantage of PCT in improving the TFR concentration, a nonlinear modulated signal is taken as an example, i.e.,

$$s(t) = 3e^{-0.05t} \sin\left(6\pi t + 6\pi t^2 - 0.5t^3\right) \quad 0 \le t \le 25 \tag{16}$$

which has exponential decay amplitude and IF law of $IF(t) = 3 + 6t - 1.5t^2/2\pi$. The sampling frequency is set to 100 Hz. The signal is contaminated by the white Gaussian noise. The SNR is of -6 dB. The TFR obtained by STFT, wavelet transform (WT), WVD, adaptive STFT (ASTFT) [4], reassigned spectrogram, reassigned pseudo WVD, chirplet transform, and PCT are shown in Fig. 4. Hereinafter, without special note, the window length is

set to 1024. ASTFT applies an adaptation rule of maximum correlation criterion. The reassigned spectrogram and reassigned pseudo WVD refers to [42].The chirp rate of chirplet transform is 5 Hz/s and the parameters applied by PCT is $(6, -1.5/2\pi)$.

It can be seen that the STFT and WT cannot provide concentrated TFR because of the signal-independent time- frequency resolution (see Fig. 4(a) and (b)). The WVD is sensitive to noise, and the undesired cross-terms are troublesome for the better interpretation of TFR (see Fig. 4(c)). The ASTFT applies signal-driven window size, i.e., the shorter window is used when IF varies quickly with time, while longer window when frequency content slowly changes. Despite of this, the concentration of the obtained TFR is still not satisfying. Moreover, it is difficult to select proper window length after 17 s when the signal attenuates significantly (see Fig. 4(d)). The reassigned technique assigns the average of energy in a domain to the nearby sampling point of the gravity center of these energy contributions. (see Fig. 4(e) and (f)). However, the concentration of the reassigned spectrogram is fairly improved as shown in Fig. 4(e) due to the poor concentration of the pre-reassigned spectrogram. Moreover, the reassigned technique introduces spurious points that are not likely to be associated to the given signal with the interference of noise. Fig. 4(g) shows that the chirplet transform, with a single chirp rate, could only characterize the time-frequency signature locally. Meanwhile, the energies of other frequency contents are smeared both in time and frequency. The most concentrated TFR is generated by the PCT, as shown in Fig. 4(h). This example proves that PCT is not only capable of characterizing accurate nonlinear IF of signal but also preserving the real energy distribution even when the signal has obvious attenuation.

B. Spline Chirplet Transform [38]

Although the polynomial chirplet transform shows advantage in analyzing nonlinear modulated signal, it is not suitable to analyze signals with complex IF in long interval. Such signals might require polynomial of high degree to characterize its IF. However, polynomial approximation suffers "Runge" phenomenon when polynomials of high degree are used. To avoid "Runge" phenomenon, an attractive solution is to use piece-wise polynomial of low degree, i.e., spline function. When kernel function, $\kappa_{\mathbf{P}}(t)$, is replaced with a spline function, and substituted into (7), we can obtain

$$\begin{aligned} &SCT(t_0,\omega;\mathbf{C}) \\ &= \int_{-\infty}^{+\infty} z(\tau)\,\Phi_{\mathbf{C}}^{R}(\tau)\,\Phi_{t_0,\mathbf{C}}^{S}(\tau)\,w_\sigma^*(\tau-t_0)\,e^{-j\omega\tau}d\tau, \\ &t_0 \in [t_l, t_{l+1}] \\ &\Phi_{\mathbf{C}}^{R}(\tau) = e^{-j\sum_{i=1}^{n}\frac{C_{l,i}}{i}(\tau-t_l)^i+o_l} \\ &\Phi_{t_0,\mathbf{C}}^{S}(\tau) = e^{j\tau\cdot\sum_{i=1}^{n}C_{l,i}(t_0-t_l)^{i-1}} \end{aligned} \tag{17}$$

where t_l denotes the lth knot of spline function, and $-\infty = t_0 < t_1 < \cdots < t_N < t_{N+1} = \infty$, N is the total number of spline knots; $\mathbf{C} = \{C_{l,i}\}$ is parameter matrix; o_l is integration constant given by

$$o_l - o_{l+1} = \sum_{i=1}^{n}\frac{C_{l+1,i}}{i}(t_l - t_{l+1})^i. \tag{18}$$

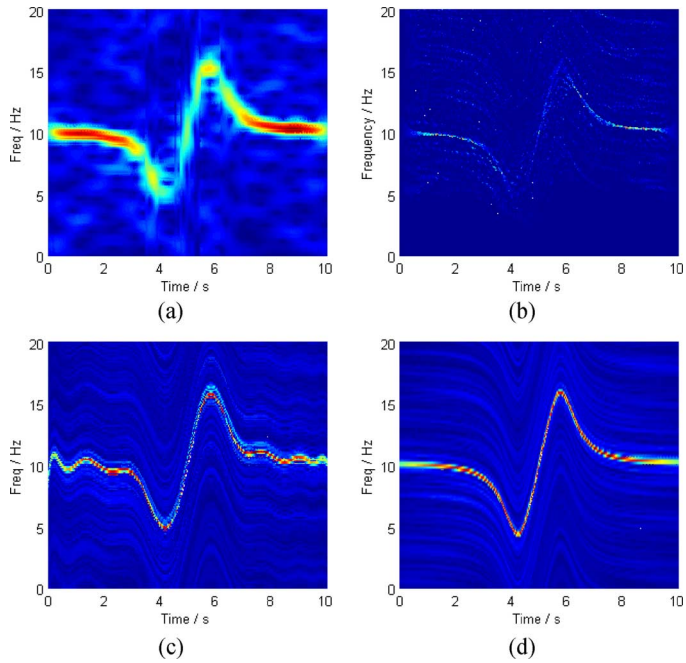

Fig. 5. TFRs of the signal in (19). (a) ASTFT. (b) reassigned pseudo WVD. (c) PCT. (d) SCT.

Equation (17) is named spline chirplet transform (SCT). To illustrate the advantage of SCT using spline kernel, a non-stationary signal is taken as an example, i.e.,

$$s(t) = \sin\left\{20\pi t + 10\pi \arctan\left[(t-5)^2\right]\right\}, 0 \le t \le 10\ \mathrm{s} \tag{19}$$

whose IF law is $IF(t) = \frac{10(t-5)}{1+(t-5)^4} + 10$. The sampling frequency is set to 100 Hz. The SNR is -2 dB.

The TFRs obtained by ASTFT, reassigned pseudo WVD, PCT and SCT are shown in Fig. 5. The PCT uses a polynomial kernel of 24 degree, while the SCT applies 4 degree spline kernel with 24 breaks. The parameters of the two kernels can be obtained by approximating the real IF with polynomial and spline respectively. For the sake of saving space, these parameters applied are not listed.

In Fig. 5(a), it can be seen that although the ASTFT applies signal-dependent window length, the obtained TFR is still not well concentrated. Reassigned pseudo WVD suppresses the cross-term introduced by WVD, though the reassignment introduces pseudo term since the computed gravity center interfered by noise and adjacent frequency contents, especially between 4 s and 6 s (see Fig. 5(b)). For this signal, PCT suffers "Runge" phenomenon so that the obtained TFR cannot describe the correct IF of the signal (see Fig. 5(c)). In fact, there is no available parameters that can make PCT characterize the real IF accurately in this case. On the other hand, the best TFR is generated by the SCT, as shown in Fig. 5(d).

The example implies that SCT could avoid "Runge" phenomenon by using piece-wise polynomial with low degree. The spline kernel formulation enables SCT to deal with the signal whose IF cannot be approximated by a polynomial. Therefore, the SCT is suitable to analyze non-stationary signals with complex IF in long interval.

C. Generalized Warblet Transform [40]

The warblet transform has been proposed to deal with signals with periodic IF [38]. However, it is not suitable to analyze signals with non-periodic IF. To overcome such a deficiency, kernel function, $\kappa_{\mathbf{P}}(t)$, is replaced with Fourier series, so that we can obtain

$$GWT_s(t_0,\omega;\mathbf{a},\mathbf{b},\mathbf{fm}) = \int_{-\infty}^{\infty} z(\tau)\,\Phi^R_{\mathbf{a},\mathbf{b},\mathbf{fm}}(\tau)\,\Phi^S_{t_0,\mathbf{a},\mathbf{b},\mathbf{fm}}(\tau)\,w^*_\sigma(\tau-t_0)\,e^{-j\omega\tau}d\tau \tag{20}$$

with

$$\Phi^R_{\mathbf{a},\mathbf{b},\mathbf{fm}}(\tau) = e^{-j\left[\sum_{i=1}^{\mathfrak{A}}\frac{a_i}{fm_i}\cos(2\pi\cdot fm_i\cdot\tau)+\sum_{i=1}^{\mathfrak{A}}\frac{b_i}{fm_i}\sin(2\pi\cdot fm_i\cdot\tau)\right]}$$

$$\Phi^S_{t_0,\mathbf{a},\mathbf{b},\mathbf{fm}}(\tau) = e^{j2\pi\tau\left[-\sum_{i=1}^{\mathfrak{A}}a_i\sin(2\pi\cdot fm_i\cdot t_0)+\sum_{i=1}^{\mathfrak{A}}b_i\cos(2\pi\cdot fm_i\cdot t_0)\right]}$$

where $\mathfrak{A}$ denotes the order of Fourier series; $\mathbf{a}=\{a_1,a_2,\ldots,a_{\mathfrak{A}}\}$, $\mathbf{b}=\{b_1,b_2,\ldots,b_{\mathfrak{A}}\}$ and $\mathbf{fm}=\{fm_1,fm_2,\ldots,fm_{\mathfrak{A}}\}$ denote coefficients of sine series, cosine series, as well as the frequencies of harmonics, respectively.

Equation (20) is named generalized warblet transform (GWT). Here, a non-stationary signal is taken as an example, i.e., see equation (21) at the bottom of the page.

The IF law of the signal is

$$IF(t) = 10+\frac{24}{\pi}\left[\sin(t)+\frac{1}{3}\sin(3t)+\frac{1}{5}\sin(5t)+\frac{1}{7}\sin(7t)\right]$$

The sampling frequency is set to 100 Hz and the SNR is -4 dB. The obtained TFRs are shown in Fig. 6. The parameters of the GWT is set to $\{fm_1,fm_2,\ldots,fm_6\}=1/2\pi\{1,2,3,4,5,7\}$, $\{b_1,b_2,\ldots,b_6\}=\{0,\ldots,0\}$ and $\{a_1,a_2,\ldots,a_6\}=\{-24/\pi,0,-8/\pi,0,-24/5\pi,0,-24/7\pi\}$. The parameters of the SCT can be obtained by approximating the real IF with Fourier series, which are not listed for saving space.

From Fig. 6(a) and (b), it can be seen that both ASTFT and reassigned pseudo WVD cannot provide accurate TFR for the signal. On contrast, the SCT and the GWT could achieve the most concentrated TFR as shown in Fig. 6(c) and (d). In particular, the GWT manages to use fewer parameters to reach the same performance as the SCT.

Another example is the signal in (16). The TFR obtained by the GWT is the same as Fig. 4(h). Although a great number of terms are required to approximate the non-periodic IF, the GWT still provides a well concentrated TFR in this case. This is because any continuous function can be decomposed into Fourier series. The examples imply that GWT is also able to analyze signals with periodic or non-periodic IF.

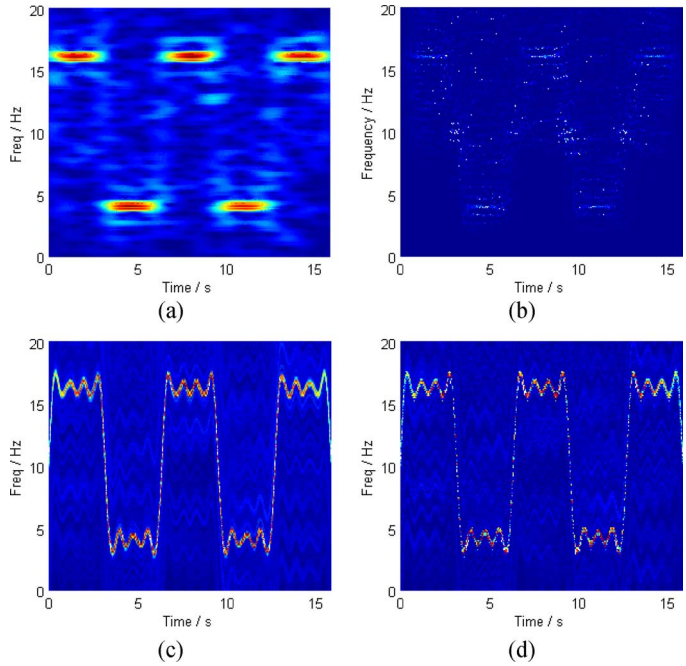

Fig. 6. TFRs of the signal in (21). (a) ASTFT. (b) reassigned pseudo WVD. (c) SCT. (d) WCT.

D. Polynomial Localized Frequency Delay Transform

As a counterpart of the PCT, we replace kernel function in the dual definition of the GPTF transform, $\gamma_{\mathbf{Q}}(\omega)$, with polynomial function of frequency. Therefore, we can obtain

$$PLFDT_{\hat{s}}(t,\omega_0;q_1,q_2,\ldots,q_n) = \frac{1}{2\pi}\int_{-\infty}^{+\infty}\overline{Z}_{q_1,q_2,\ldots,q_n}(\theta)\,\hat{w}^*_\sigma(\theta-\omega_0)\,e^{-j\theta t}d\theta \tag{22}$$

with

$$\overline{Z}_{q_1,q_2,\ldots,q_n}(\theta) = \hat{s}(\theta)\cdot\Gamma^R_{q_1,q_2,\ldots,q_n}(\theta)\cdot\Gamma^S_{\omega_0,q_1,q_2,\ldots,q_n}(\theta),$$

$$\Gamma^R_{q_1,q_2,\ldots,q_n}(\theta) = e^{-j\sum_{i=2}^{n+1}\frac{1}{i}q_{i-1}\theta^i}$$

$$\Gamma^S_{\omega_0,q_1,q_2,\ldots,q_n}(\theta) = e^{j\theta\cdot\sum_{i=2}^{n+1}q_{i-1}\omega_0^{i-1}}$$

where $\{q_1,q_2,\ldots,q_n\}$ denotes polynomial coefficients. Equation (22) is named polynomial localized frequency delay transform (PLFDT). Similar to the PCT, PLFDT is able to analyze signals with any continuous localized frequency delay, yet still suffers "Runge" phenomenon.

$$s(t) = \sin\left\{20\pi t - 48\left[\cos(t)+\frac{1}{9}\cos(3t)+\frac{1}{25}\cos(5t)+\frac{1}{49}\cos(7t)\right]\right\} \tag{21}$$

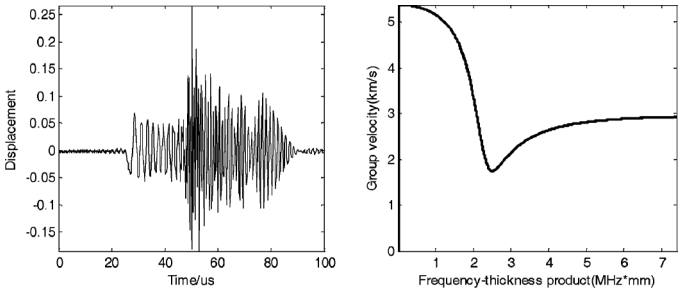

Fig. 7. S0 mode Lamb wave. (a) Time domain signal. (b) group velocity.

E. Fourier Series Localized Frequency Delay Transform

As a counterpart of the GWT, we replace the kernel function in the dual definition of the GPTF transform, $\gamma_{\mathbf{Q}}(\omega)$, with Fourier series. Thus, we can obtain

$$FLFDT_{\hat{s}}\left(t,\omega_0;\hat{\mathbf{a}},\hat{\mathbf{b}},\mathbf{f}\hat{\mathbf{m}}\right) = \frac{1}{2\pi}\int_{-\infty}^{+\infty}\overline{Z}_{\hat{\mathbf{a}},\hat{\mathbf{b}},\mathbf{f}\hat{\mathbf{m}}}(\theta)\,\hat{w}_{\sigma}^{*}(\theta-\omega_0)\,e^{-j\theta t}d\theta \quad (23)$$

with

$$\overline{Z}_{\hat{a},\hat{b},f\hat{m}}(\theta) = \hat{s}(\theta)\cdot\Gamma^{R}_{\hat{\mathbf{a}},\hat{\mathbf{b}},\mathbf{f}\hat{\mathbf{m}}}(\theta)\cdot\Gamma^{S}_{\omega_0,\hat{\mathbf{a}},\hat{\mathbf{b}},\mathbf{f}\hat{\mathbf{m}}}(\theta)$$

$$\Gamma^{R}_{\hat{\mathbf{a}},\hat{\mathbf{b}},\mathbf{f}\hat{\mathbf{m}}}(\theta) = e^{-j\left[\sum_{i=1}^{\mathfrak{A}}\frac{\hat{a}_i}{f\hat{m}_i}\cos(2\pi\cdot f\hat{m}_i\cdot\theta)+\sum_{i=1}^{\mathfrak{A}}\frac{\hat{b}_i}{f\hat{m}_i}\sin(2\pi\cdot f\hat{m}_i\cdot\theta)\right]}$$

$$\Gamma^{S}_{\omega_0,\hat{\mathbf{a}},\hat{\mathbf{b}},\mathbf{f}\hat{\mathbf{m}}}(\theta) = e^{j\theta\left[-\sum_{i=1}^{\mathfrak{A}}\hat{a}_i\sin(2\pi\cdot f\hat{m}_i\cdot\omega_0)+\sum_{i=1}^{\mathfrak{A}}\hat{b}_i\cos(2\pi\cdot f\hat{m}_i\cdot\omega_0)\right]}$$

Equation (23) is named localized frequency delay transform (FLFDT).

To illustrate the performance of PLFDT and FLFDT, Lamb wave signal is adopted as an example. Lamb wave signal is a classical guided wave, each mode of which processes nonlinear group velocity. For example, the waveform of S0 mode lamb wave is shown in Fig. 7(a), whose group delay curve is shown in Fig. 7(b). The simulated signal was add with White Gauss ion noise and the SNR is of -2.2 dB.

The TFRs obtained by ASTFT, reassigned pseudo WVD, PLFDT and FLFDT are shown in Fig. 8. The PCT uses polynomial of 26 degree. Parameters of the PCT and the GWT can be obtained by approximating the real LFD with polynomial, and applying Fourier transform on real LFD respectively, both of which are not listed for saving space. It can be seen that the ASTFT and the reassigned pseudo WVD fail to characterize the real localized frequency delay of the signal for poor concentration and pseudo terms respectively (see Fig. 8(a) and (b)). In Fig. 8(c), it is clear to see that the PLFDT suffers "Runge" phenomenon. On the other hand, the FLFDT avoids this problem and is more powerful to characterize the time-frequency signature of S0 mode wave signal as shown in Fig. 8(d).

To sum up, three promising kernels have been detailed discussed. The pros and coms of these parameterized kernel formulations are summarized in Table II.

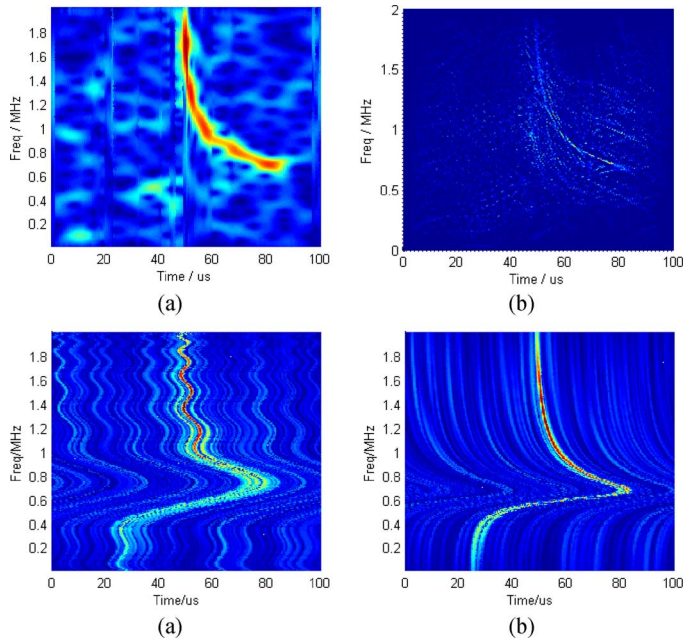

Fig. 8. TFR of the S0 mode Lamb wave signal. (a) ASTFT. (b) reassigned pseudo WVD. (a) PLFDT. (b) FLFDT.

TABLE II
SUMMARY OF THREE KERNEL FORMULATIONS

kernel	*Pros*	*Cons*
polynomial	suitable for signals with any continuous IF/LFD in short interval	suffers from "Runge" phenomenon
spline	suitable for signals with any complex IF/LFD in long interval	need plenty of polynomial pieces when IF/LFD is highly dynamic
Fourier series	suitable for signals with periodic and non-periodic IF/LFD in long interval	need plenty of sine/cosine terms when IF/LFD is non-periodic

V. KERNEL IDENTIFICATION

According to the characteristic of GPTF transform, a TFR of better concentration can be generated by using better matched kernel. Highly concentrated TFR is able to characterize accurate time-frequency signature of signal. The TFR peak is an estimation of the time-frequency signature. Therefore, we develop a kernel identification method based on recursive approximation of the TFR ridge. Specifically, in the each iteration, the kernel is identified by approximating the extracted TFR ridge. Then, the identified kernel is fed into GPTF transform to generate an improved TFR. The detailed procedure is illustrated in Fig. 9, where $\mathbf{P}_i$ denotes the parameter settings in the ith iteration. $\widetilde{IF}_i(t)$ stands for estimated IF in the ith iteration, which is the extracted TFR ridge. $\overline{\overline{IF}}_i(t)$ is the fitting curve in the ith iteration. $\tilde{\mathbf{P}}_i$ is the estimated parameters. The terminating condition is given by

$$\Lambda_i = mean\left(\int\frac{\left|\widetilde{IF}_i(t)-\widetilde{IF}_{i-1}(t)\right|}{\left|\widetilde{IF}_i(t)\right|}dt\right) < \zeta \quad (24)$$

where ζ is a minor constant, and $\widetilde{F}_0(t)=0$.

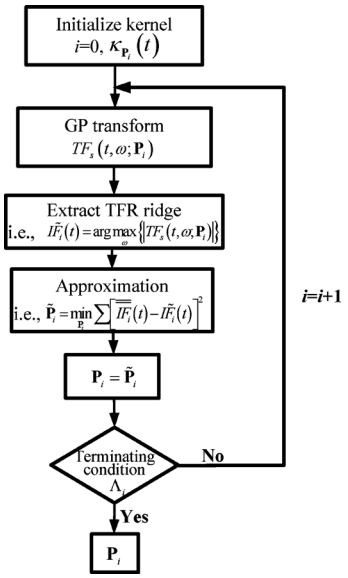

Fig. 9. Kernel identification based on recursive approximation of TFR ridge.

Compared to extracting TFR ridge in one trail, the recursive approximation of the TFR ridge (RA-TFR) is expected to be more effective for kernel identification. In particular, two questions are dominant during the recursive approximation: 1) selecting proper initial TFR; 2) curve fitting subject to desired constraints. First, the initial TFR is required to have less cross-term and acceptable concentration. The better initial TFR can catalyze the kernel identification. Here, we apply $\kappa_{\mathbf{P}_0}(t) = 0$ so that the initial GPTF transform equals to the short-time Fourier transform (STFT). It is probably not the best choice in every case, but is reasonable to automatically implement the GPTF transform. Second, since poor concentration and noise may distort the extraction of the TFR ridge, the curve fitting needs to balance the tradeoff between bias and variance.

In the kernel identification procedure, the IF estimation is of paramount importance to be considered. And the convergence criteria can be determined whether the bias of the IF estimation error is becoming smaller after each iteration. Assuming the phase of the original signal can be modeled by the function $\phi(t)$ with determined parameter P, denoting to $\phi(t,\mathbf{P})$, the estimated phase function in the ith iteration is $r_i(t) = \phi(t,\mathbf{P}_i)$. The bias of the estimated IF error $\Delta\widetilde{IF}_i(t)$ from detecting the ridge of the TFR is given by [43]

$$Bias\left\{\Delta\widetilde{IF}_i(t)\right\} \rightarrow \sum_{k=1}^{+\infty}\frac{\left[\phi^{(2k+1)}(t)-r_i^{(2k+1)}(t)\right]\sigma^{2k}M_{1,2k+2}}{(2k+1)!M_{1,2}} \quad (25)$$

where

$$M_{m,k}=\int_{-\infty}^{+\infty}t^k w_\sigma^m(t)\,dt$$

If the following conditions are satisfied for $i=\mathrm{I}$, see equation (26) at the bottom of the page, then the bias of the IF estimation error based on the TFR of the ith GPTF transform iteration, will be smaller than the bias of $\Delta\widetilde{IF}(t)$ from the initialized step [43]. Thus, the estimated IF is closer to the true IF than the initial estimated IF $r_1'(t) = \phi'(t,\mathbf{P}_1)$ for $t\in\mathbb{R}$. Meanwhile, the estimated parameters P_{I+1} is closer to the actual parameters P. The above conditions are further satisfied for $i=I+1$, and the bias of the corresponding IF estimation error $\Delta\widetilde{IF}_{I+1}(t)$ is further smaller than the bias of $\Delta\widetilde{IF}_I(t)$. In this case, the implementation of the iterative procedure will finally converge to true IF.

To illustrate the effectiveness of RA-TFR based method, we use PCT, one instance of the GPTF transform, as an example. The PCT is the GPTF transform that applies a polynomial kernel. For example, a signal is given by

$$s(t)=\sin\left[2\pi\left(10t+\frac{5}{4}t^2+\frac{1}{9}t^3-\frac{1}{160}t^4\right)\right] \quad (27)$$

whose IF law is $IF(t) = 10+2.5t+t^2/3-t^3/40$. The sampling frequency is set to 100 Hz. In this case, the signal is seriously contaminated by a white noise with SNR of -1 dB. In each approximation step, least square method and polynomial function of order 4 are used, such that

$$IF(t)\approx c_0+\sum_{k=1}^{4}c_k t^k \quad (28)$$

The window size is set to 512 and the terminating condition is set to 0.05. Before reaching the criterion, 4 cycles are conducted. Figs. 10–12 show the TFR, the extracted ridge and its polynomial fitting after the first, second and last time PCT. It can be seen that as the concentration of TFR improves, polynomial approximation of the extracted ridge becomes closer to the real IF of the signal. It can be also noticed that the distortion in the extracted ridge caused by noise is removed during the recursive approximation. The computed terminating conditions are listed in Table III. Relative error between the real and estimated IF is used to evaluate the accuracy of IF estimation. Table IV lists relative error in each step. The identified kernel parameters in the each iteration are listed in Table V. It can be seen that the estimated parameters are approaching the real value during the recursive approximation.

$$Error = mean\left(\int\left|\frac{\widetilde{IF}_i(t)-IF(t)}{IF(t)}\right|dt\right) \quad (29)$$

$$0<\sum_{n=-\infty}^{+\infty}w_\sigma(nT)nT\left|\phi_i(t+nT)-\phi_i'(t)\,nT-r_i(t+nT)+r_i'(t)\,nT\right| \quad (26)$$

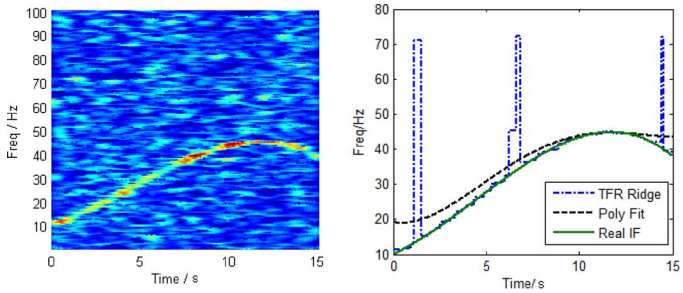

Fig. 10. After 1st time PCT(STFT). (a) TFR. (b) extracted ridge and polynomial fitting.

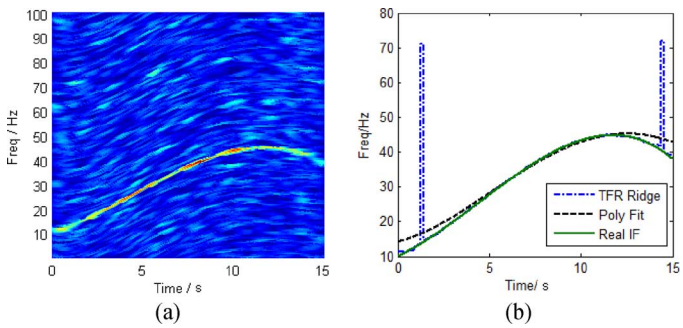

Fig. 11. After 2nd time PCT. (a) TFR. (b) extracted ridge and polynomial fitting.

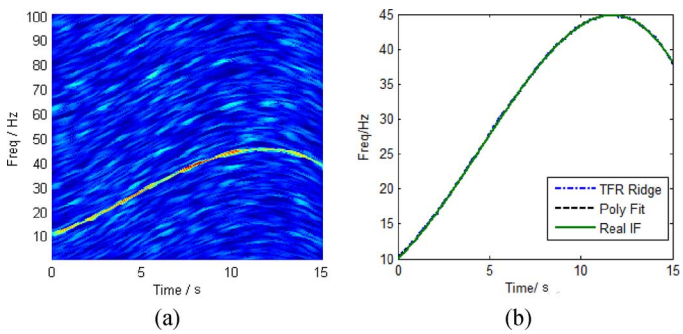

Fig. 12. After the last time PCT. (a) TFR. (b) extracted ridge and polynomial fitting.

TABLE III
TERMINATING CONDITIONS OF KERNEL IDENTIFICATION BY USING PCT

$(i, i+1)$	(1, 2)	(2, 3)	(3, 4)
Λ_i	9.13	1.06	0.06

TABLE IV
RELATIVE ERROR BETWEEN REAL AND ESTIMATED IF

i	i=1	i=2	i=3	i=4
Error (%)	9.27	4.18	2.74	1.44

It can be seen that the burst errors from the ridge detection as shown in Fig. 10(b) cannot affect the kernel parameters. This example verifies the effectiveness of the RA-TFR based method in providing accurate kernel identification for signals with slowly varying IF. If the signal has rapidly varying IF, high-order polynomial or spline kernel is preferred. For example, a signal is given as

TABLE V
IDENTIFIED KERNEL PARAMETERS BY USING PCT

	1	2	3	4	Real value
$\tilde{c}_0$	9.20	9.86	10.01	10.00	10.00
$\tilde{c}_1$	1.69	2.62	2.47	2.51	2.50
$\tilde{c}_2$	1.43	0.32	0.34	0.33	0.33
$\tilde{c}_3$	-0.19	-0.03	-0.03	-0.02	-0.03
$\tilde{c}_4$	0.01	0.03e-2	0.01e-2	0.04e-9	0.01e-12

$$s(t) = \sin\left[15\pi t + 3\pi t^2 + 12\pi \sin(2t)\right], 0 \le t \le 10 \quad (30)$$

The true IF law of the signal is $\mathrm{IF}(t) = 7.5 + 3t + 12\cos(2t)$. The sampling frequency is set to 150 Hz. The SNR of the signal is -1 dB. Window size is set to 512 and the terminating condition is set to 0.05. Before reaching the criterion, 6 cycles are conducted. Figs. 13–15 show the results of the 1st, 3rd, and 6th iteration for saving the space. In this case, the 17-order kernel polynomial is applied and the estimated polynomial coefficients after the 11th order are close to zero. It is noticed that using the high-order polynomial for the signal with such rapidly varying IF, the burst errors from ridge detection shown in Fig. 13(b) still do not affect the estimation result of kernel parameters.

For the signal with discontinuous IF, the spline kernel could be applied by treating the discontinuity points as an unconnected knot. In this case, the smooth condition at such knot needs to be redefined and the original spline is break into disconnected pieces. The RA-TFR method is still effective for such signals, while the SCI based method might need prior knowledge about these discontinuity points. For the detail about the utilization of the spline kernel, interested readers could refer to [44].

This method can be easily adopted by any kind of GPTF transforms. The attention needs to be paid on the approximation with the different kernel forms. For example, when the SCT is considered, the B-spline is used to fit the extracted ridge. While Fourier transform of the extracted ridge can be used to identify the parameters for the GWT. It is worth mentioning that the polynomial function order can be determined by trial. Usually, a relatively large order can be adopted for the polynomial function at beginning. If the extracted TFR peak data can be well approximated with a polynomial function of relative low order, then the estimated high order polynomial coefficients would be close to zero.

Ideally, the finer resolution leads to the better concentration of the TFR. The resolution of the initial TFR (STFT) is limited by the uncertainty principle. Determining an optimal window length is an open question in the application of the STFT. The best window length for a particular signal depends on the signal itself. In our study, the window length is recommended to be relatively short in the initialized step in order to obtain the average time and frequency resolution, yet it should not be so short that substantially different frequency contents are included; while the longer window is more suitable for the following recursive transforms to achieve the better concentration.

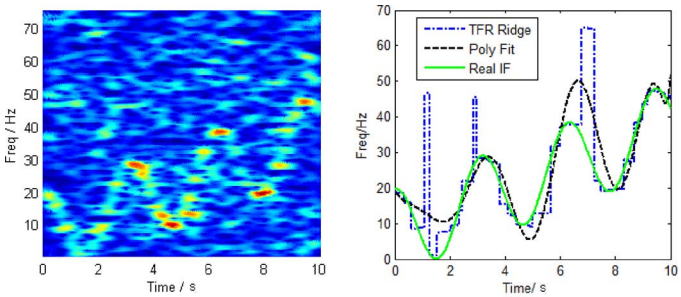

Fig. 13. After 1st time PCT(STFT). (a) TFR. (b) extracted ridge and polynomial fitting.

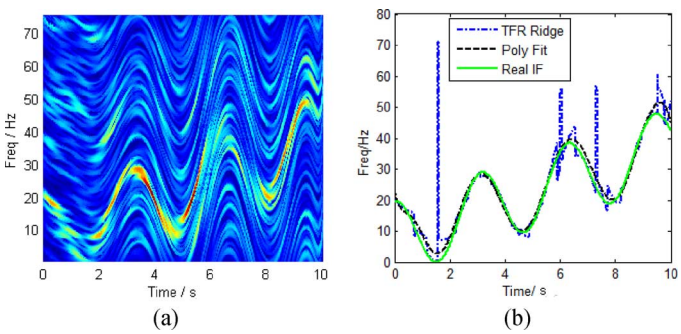

Fig. 14. After 3rd time PCT. (a) TFR. (b) extracted ridge and polynomial fitting.

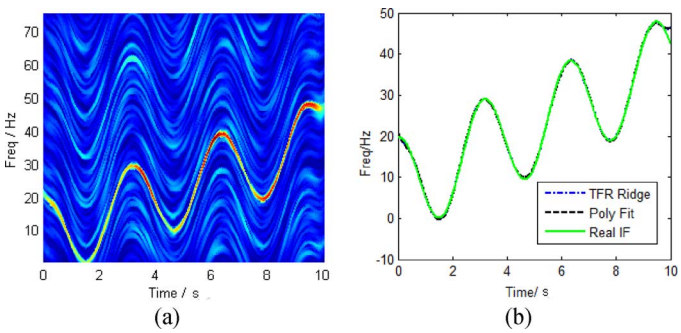

Fig. 15. After 6rd time PCT. (a) TFR. (b) extracted ridge and polynomial fitting.

Furthermore, in the case of multi- component signal whose components have the same frequency modulation law and the different amplitudes, only the ridge of the dominant component is needed to identify the kernel. For example, based on signal in (27), constructing a multi-component signal as

$$s(t) = \sin\left[2\pi\left(10t + \frac{5}{4}t^2 + \frac{1}{9}t^3 - \frac{1}{160}t^4\right)\right] + 0.7\sin\left[2\pi\left(14t + \frac{5}{4}t^2 + \frac{1}{9}t^3 - \frac{1}{160}t^4\right)\right] \quad (31)$$

whose IF laws of the two components are $IF1(t) = 10 + 2.5t + t^2/3 - t^3/40$ and $IF2(t) = 14 + 2.5t + t^2/3 - t^3/40$, respectively. The sampling frequency is set to 100 Hz and the SNR is -1 dB. Figs. 16 and 17 are the results of the 1st and 7th time PCT. It can be seen that the kernel can be well estimated and the final TFR achieves the satisfied concentration for the two components. At this point, the multi-component signal analysis is equivalent to the analysis of the mono-component signal.

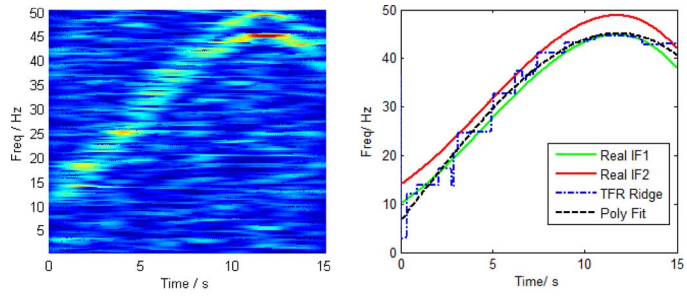

Fig. 16. After 1st time PCT. (a) TFR. (b) extracted ridge and polynomial fitting.

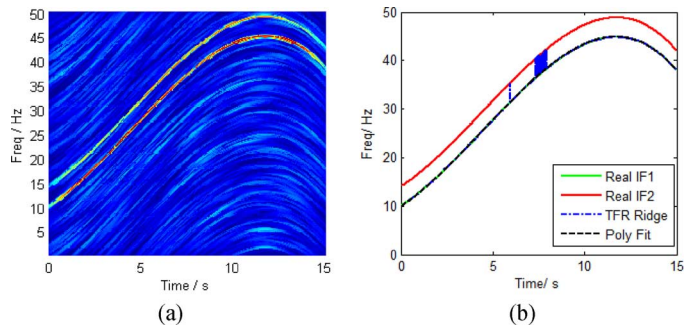

Fig. 17. After 7th time PCT. (a) TFR. (b) extracted ridge and polynomial fitting.

When the components have the same frequency modulation law and amplitudes or have the different frequency modulation laws, the ridges of all components have to be extracted from the initial TFR respectively. It usually requires heuristic masking techniques based on the prior knowledge [45]. On the other hand, the non-TFR based signal parameter estimators are candidates for identifying the kernel parameters and combining with the GPTF to analyze multi-component signals, which is beyond the scope of this paper. Interest readers please refer to [46], [47].

VI. Conclusion

In this paper, we defined a general parameterized time – frequency transform (GPTF transform). It applies generalized kernel based rotation operator and shift operator. The GPTF transform is proved to have several properties, i.e., linearity, scaling, time shifting and frequency shifting. Based on the kernel base definition, its dual definition in frequency domain is proposed as well. The usage of general kernel in GPTF transform provides the availability of analyzing signal with different time-frequency signature. Moreover, by adopting promising kernel, more powerful time-frequency transform can be constructed the same standpoint. Short-time Fourier transform, short-frequency Fourier transform, chirplet transform, warblet transform and FM^{m}let transform are all special instances of GPTF transform. In addition, five parameterized time-frequency transforms are constructed, i.e., the polynomial chirplet transform, the spline chirplet transform, the generalized warblet transform, the polynomial localized frequency delay transform and the Fourier series localized frequency delay

transform. The analysis results show that the GPTF transform, with properly formulated kernel function, is able to accurately characterize the time-frequency signature of various non-stationary signals. In addition, we proposed an effective kernel identification method for the desired GPTF. The results verify that the proposed method is able to facilitate the determination of the kernel for the GPTF in real practice.

REFERENCES

[1] J. Ville, "Theorie et application de la notion de signal analytic," *Cables et Transmessions[J]*, vol. 93, pp. 61–74, 1948.

[2] L. Cohen, "Generalized phase-space distributions," *J. Math. Phys.*, vol. 7, pp. 781–786, 1966.

[3] F. Auger and P. Flandrin, "The why and how of time-frequency reassignment," in *Proc. IEEE-SP Internat. Symp. Time-Frequency Time-Scale Ana.*, 1994, pp. 197–200.

[4] H. K. Kwok and D. L. Jones, "Improved instantaneous frequency estimation using an adaptive short-time Fourier transform," *IEEE Trans. Signal Process.*, vol. 48, no. 10, pp. 2964–2972, Oct. 2000.

[5] B. Liu, S. Riemenschneider, and Z. Shen, "An adaptive time-frequency representation and its fast implementation," *J. Vibration Acoust.*, vol. 129, no. 2, pp. 1–24, 2007.

[6] J. Zhong and Y. Huang, "Time-frequency representation based on an adaptive short-time Fourier transform," *IEEE Trans. Signal Process.*, vol. 58, no. 10, pp. 5118–5128, Oct. 2010.

[7] S. C. Pei and S. G. Huang, "STFT with adaptive window width based on the chirp rate," *IEEE Trans. Signal Process.*, vol. 60, no. 8, pp. 4065–4080, Aug. 2012.

[8] V. Katkovnik, "A new method for varying adaptive bandwidth selection," *IEEE Trans. Signal Process.*, vol. 47, no. 9, pp. 2567–2571, Sep. 1999.

[9] C. S. Burrus *et al., Introduction to Wavelets and Wavelet Transforms: A Primer*. Upper Saddle River, NJ, USA: Prentice hHall, 1998, vol. 23.

[10] R. G. Stockwell, L. Mansinha, and R. P. Lowe, "Localization of the complex spectrum: The S transform," *IEEE Trans. Signal Process.*, vol. 44, no. 4, pp. 998–1001, Apr. 1996.

[11] M. Unser, A. Aldroubi, and M. Eden, "A family of polynomial spline wavelet transforms," *Signal Process.*, vol. 30, no. 2, pp. 141–162, 1993.

[12] J. Lerga and V. Sucic, "Nonlinear IF estimation based on the pseudo WVD adapted using the improved sliding pairwise ICI rule," *IEEE Signal Process. Lett.*, vol. 16, no. 11, pp. 953–956, 2009.

[13] P. Flandrin and O. Rioul, "Affine smoothing of the Wigner-Ville distribution," in *Proc. IEEE Intern. Conf. Acoust., Speech, Signal Process.*, 1990, pp. 2455–2458.

[14] L. Stankovic and V. Katkovnik, "Instantaneous frequency estimation using higher order L-Wigner distributions with data-driven order and window length," *IEEE Trans. Inf. Theory*, vol. 46, no. 1, pp. 302–311, Jan. 2000.

[15] F. Auger and P. Flandrin, "Improving the readability of time–frequency and time-scale representations by the reassignment method," *IEEE Trans. SignalProcess.*, vol. 43, no. 5, pp. 1068–1089, May 1995.

[16] P. Flandrin, F. Auger, and E. Chassande-Mottin, "Time-frequency reassignment: From priciples to algorithms," *Appl. Time-Frequency Signal Process.*, vol. 5, pp. 179–203, 2003.

[17] S. Mann and S. Haykin, "'Chirplets' and 'warblets': Novel time-frequency methods," *Electron. Lett.*, vol. 28, no. 2, pp. 114–116, 1992.

[18] D. Mihovilovic and R. Bracewell, "Adaptive chirplet representation of signals on time-frequency plane," *Electron. Lett.*, vol. 27, no. 13, pp. 1159–1161, 1991.

[19] S. G. Mallat and Z. Zhang, "Matching pursuits with time-frequency dictionaries," *IEEE Trans. Signal Process.*, vol. 41, no. 12, pp. 3397–3415, Dec. 1993.

[20] R. Gribonval, "Fast matching pursuit with a multiscale dictionary of Gaussian chirps," *IEEE Trans. Signal Process.*, vol. 49, no. 5, pp. 994–1001, May 2001.

[21] J. Li and H. Ling, "Application of adaptive chirplet representation for ISAR feature extraction from targets with rotation parts," *IEE Proc.-Radar, Sonar Navig.*, vol. 150, no. 4, pp. 284–291, 2003.

[22] Z. Zeng, F. Wu, L. Huang, F. Liu, and J. Sun, "The adaptive chirplet transform and its application in GPR target detection," *Appl. Geophys.*, vol. 6, no. 2, pp. 192–200, 2009.

[23] J. Li and H. Ling, "Application of adaptive chirplet representation for ISAR feature extraction from targets with rotation parts," *IEE Proc.-Radar, Sonar Navig.*, vol. 150, no. 4, pp. 284–291, 2003.

[24] Q. Yin, S. Qian, and A. Feng, "A fast refinement for adaptive Gaussian chirplet decomposition," *IEEE Trans. Signal Process.*, vol. 50, no. 6, pp. 1298–1306, Jun., 2002.

[25] Y. Lu, R. Demirli, G. Cardoso, and J. Saniie, "A successive parameter estimation algorithm for chirplet signal decomposition," *IEEE Trans. Ultrasonics, Ferroelectrics Frequency Control*, vol. 53, no. 11, pp. 2121–2131, Nov. 2006.

[26] J. Cui, W. Wong, and S. Mann, "Time-frequency analysis of visual evoked potentials using chirplet transform," *Electron. Lett.*, vol. 41, no. 4, pp. 217–218, 2005.

[27] J. Cui and W. Wong, "Investigation of short-term changes in visual evoked potentials with windowed adaptive chirplet transform," *IEEE Trans. Biomed. Eng.*, vol. 55, no. 4, pp. 1449–1454, Apr. 2008.

[28] E. Chassande-Mottin and A. Pai, "Best chirplet chain: Near-optimal detection of gravitational wave chirps," *Phys. Rev. D*, vol. 73, no. 4, pp. 1–23, 2006.

[29] B. Dugnol, C. Fernández, G. Galiano, and J. Velasco, "On a chirplet transform-based method applied to separating and counting wolf howls," *Signal Process.*, vol. 88, no. 7, pp. 1817–1826, 2008.

[30] E. J. Candes, P. R. Charlton, and H. Helgason, "Detecting highly oscillatory signals by chirplet path pursuit," *Appl. Comput. Harmonic Anal.*, vol. 24, no. 1, pp. 14–40, 2008.

[31] R. Gribonval, "Fast matching pursuit with a multiscale dictionary of Gaussian chirps," *IEEE Trans. Signal Process.*, vol. 49, no. 5, pp. 994–1001, May 2001.

[32] L. Angrisani and M. D'Arco, "A measurement method based on a modified version of the chirplet transform for instantaneous frequency estimation," *IEEE Trans. Instrum. Measur.*, vol. 51, no. 4, pp. 704–711, Aug. 2002.

[33] A. Papandreou-Suppappola and S. B. Suppappola, "Analysis and classification of time-varying signals with multiple time-frequency structures," *IEEE Signal Process. Lett.*, vol. 9, no. 3, pp. 92–95, Mar. 2002.

[34] H. Zou, Y. Chen, J. Zhu, Q. Dai, G. Wu, and Y. Li, "Steady-motion-based Dopplerlet transform: Application to the estimation of range and speed of a moving sound source," *IEEE J. Ocean. Eng.*, vol. 29, no. 3, pp. 887–905, Aug. 2004.

[35] H. Zou, Q. Dai, R. Wang, and Y. Li, "Parametric TFR via windowed exponential frequency modulated atoms," *IEEE Signal Process. Lett.*, vol. 8, no. 5, pp. 140–142, May 2001.

[36] V. Katkovnik, "A new form of the Fourier transform for time-varying frequency estimation," *Signal Process.*, vol. 47, no. 2, pp. 187–200, 1995.

[37] Z. K. Peng, G. Meng, F. L. Chu, Z. Q. Lang, W. M. Zhang, and Y. Yang, "Polynomial chirplet transform with application to instantaneous frequency estimation," *IEEE Trans. Instrumen. Measur.*, vol. 60, no. 9, pp. 3222–3229, Sep. 2011.

[38] Y. Yang, Z. K. Peng, G. Meng, and W. M. Zhang, "Spline-Kernelled chirplet transform for the analysis of signals with time-varying frequency and its application," *IEEE Trans. Ind. Electron.*, vol. 59, no. 3, pp. 1612–1621, Mar. 2012.

[39] L. Angrisani, M. D'Arco, R. Schiano Lo Moriello, and M. Vadursi, "On the use of the warblet transform for instantaneous frequency estimation," *IEEE Trans. Instrumen. Measur.*, vol. 54, no. 4, pp. 1374–1380, Apr. 2005.

[40] Y. Yang, Z. K. Peng, G. Meng, and W. M. Zhang, "Characterize highly oscillating frequency modulation using generalized Warblet transform," *Mechan. Syst. Signal Process.*, vol. 26, pp. 128–140, 2012.

[41] Weierstrass's Theorem. [Online]. Available: http://mathworld.wolfram.com/WeierstrassApproximationTheorem.html

[42] 1991 Free Software Foundation, Inc., "Time-Frequency Toolbox Version 1.0," Rice University, Houston, TX, USA, January 1996 Copyright (c).

[43] S. Wang *et al.*, "Matching demodulation transform and synchrosqueezing in time-frequency analysis," *IEEE Trans. Signal Process.*, vol. 62, no. 1, pp. 69–84, Jan. 2013.

[44] Y. Yang, Z. K. Peng, G. Meng, and W. M. Zhang, "Spline-kernelled chirplet transform for the analysis of signals with time-varying frequency and its application," *IEEE Trans. Ind. Electron.*, vol. 59, no. 3, pp. 1612–1621, Mar. 2012.

[45] Y. Yang, W. Zhang, Z. Peng, and G. Meng, "Multicomponent signal analysis based on polynomial chirplet transform," *IEEE Trans. on Industrial Electronics*, vol. 60, no. 9, pp. 3948–3956, 2013.

[46] B. Porat and B. Friedlander, "Accuracy analysis of estimation algorithms for parameters of multiple polynomial-phase signals," in *Proc. IEEE Int. Conf. Acoust., Speech, Signal Process.*, May 1995.

[47] S. Barbarossa, A. Scaglione, and G. B. Giannakis, "Product high-order ambiguity function for multicomponent polynomial-phase signal modeling," *IEEE Trans. Signal Process.*, vol. 46, no. 3, pp. 691–708, Mar., 1998.

Y. Yang received the B.S. and M.S. degrees in mechanical engineering from Shanghai Jiao Tong University, Shanghai, China, in 2006 and 2009, respectively, where she is currently working toward the Ph.D. degree in the Mechanical Engineering Department. She studied at the Intelligent Maintenance System Center, University of Cincinnati, Cincinnati, OH, from 2007 to 2008. She is currently with the State Key Laboratory of Mechanical System and Vibration, Shanghai Jiao Tong University. Her research interests include signal processing, system identification, machine health diagnosis, and prognostics.

Z. K. Peng received the B.Sc. and Ph.D. degrees from Tsinghua University, Beijing, China, in 1998 and 2002, respectively. From 2003 to 2004, he was with the City University of Hong Kong, Kowloon, Hong Kong, as a Research Associate, and then, he was with Cranfield University, Cranfield, U.K., as a Research Officer. After that, he was with the University of Sheffield, Sheffield, U.K., for four years. He is currently a Distinguished Professor with the State Key Laboratory of Mechanical System and Vibration, Shanghai Jiao Tong University, Shanghai, China. His main expertise relates to the subject areas of nonlinear vibration, signal processing and condition monitoring, and fault diagnosis for machines and structures.

X. J. Dong received the B.S. degree in aircraft design engineering and M.S. degree in solid mechanics from Northwestern Polytechnical University, Xi'an, China, in 1999 and 2002, respectively, and the Ph.D degree in mechanical engineering from Shanghai Jiao Tong University, Shanghai, China, in 2006. He is currently a lecturer with the Shanghai Jiao Tong University. His research interests include vibration analysis, smart structures and fatigue analysis of structures.

W. M. Zhang (M'10) received the B.S. degree in mechanical engineering and the M.S. degree in mechanical design and theories from Southern Yangtze University, Wuxi, China, in 2000 and 2003, respectively, and the Ph.D. degree in mechanical engineering from Shanghai Jiao Tong University, Shanghai, China, in 2006. He is currently a Professor with the State Key Laboratory of Mechanical System and Vibration, School of Mechanical Engineering, Shanghai Jiao Tong University. He has deep experiences in the dynamics and control for micro/nanoelectromechanical systems (MEMS/NEMS). His researches involve nonlinear dynamics and chaos control, nonlinear vibration and control, coupled parametrically excited microresonators, and the reliability analysis and assessment for MEMS/NEMS applications.

G. Meng received the Ph.D. degree from Northwestern Polytechnical University, Xi'an, China, in 1988. In 1993, He was a Professor and the Director of Vibration Engineering Institute with Northwestern Polytechnical University. From 1989 to 1993, he was also a Research Assistant with Texas A&M University, College Station, an Alexander von Humboldt Fellow with Technical University Berlin, Berlin, Germany, and a Research Fellow with New South Wales University, Sydney, Australia. From 2000 to 2008, he was with Shanghai Jiao Tong University, Shanghai, China, as the Cheung Kong Chair Professor, the Associate Dean, and the Dean of the School of Mechanical Engineering. He is currently a Professor and the Director of the State Key Laboratory of Mechanical System and Vibration, Shanghai Jiao Tong University. His research interests include dynamics and vibration control of mechanical systems, nonlinear vibration, and microelectromechanical systems.